IEEE Robotics and Automation Letters (RA-L) paper, presented at ICRA 2026, Vienna, Austria. Cite as RA-L paper.

Empirical Contact Models for Soft Spherical Robots in Drake

Micah J. Oevermann[1], Dhruv Datta[1], Dylan Hilburn[2], Derek J. Pravecek[1], Rishi Jangale[1], Aaron Villanueva[1], Robert O. Ambrose[1]

***Abstract*— Accurate dynamic modeling of soft-shelled spherical robots is challenging due to coupled rigid–soft body interactions and pressure-dependent contact behavior. This letter presents a modeling strategy for an empirically tuned pendulum-driven inflatable spherical robot. The approach combines a rigid-body dynamics engine in Drake with non-conservative effects. The robot's rigid-body model is generated from a custom URDF and augmented with interchangeable joint friction modules. Three alternative outer shell contact models are also considered: Drake's native hydroelastic contact, a pressure-dependent injected stiffness–damping model derived from isolated shell experiments, and a rigid point-contact baseline. Shell dynamics are characterized in the steering direction using a custom locking fixture, yielding empirical pressure-related frequency and damping relationships to parameterize the models. Ramp descent experiments across multiple inflation pressures validate the framework, showing that an appropriate model reduces drive velocity prediction error compared to a rigid point-contact case. The approach enables modular integration of additional dynamic effects, supports data-driven parameter tuning, and provides a reproducible pathway for accurate simulation of soft spherical robots.**

Soft Robotics; Dynamic Simulation; Contact Modeling

I. INTRODUCTION

Spherical robots are hailed as a unique exploration platform. Their internal avionics are enclosed within an outer shell that protects them from debris or other harmful substances. Multiple highly functioning prototypes have been developed and studied over the years. Ren et al. built a system that handles various environments with a custom sensor array [1]. RoboBall and Moball are two other prototypes that rely on soft outer shells. RoboBall uses a custom pneumatic spherical shell propelled by a pendulum [2]. While Moball deployed a sewn outer frame stretched between spars, it relied on wind to drive it [3].

A large amount of literature is devoted to describing the complete dynamics of spherical robots. Diouf found that most spherical robots rely on classic methods of first principles to derive their equations of motion [4]. Studies that use these methods often cite the difficulty of working with the full analytical equations [5]. Researchers have invested time looking into different modeling strategies to avoid explicitly stating the whole system dynamics either through exploiting Lie bracket symmetries [6], or system identification methods [7]. Montenegro et al. used a Coppelia simulator to study the dynamics and prototype various machine learning controllers numerically [8]. While the rigid body components are an essential foundation to modeling, it is often the non-conservative forces that arise through actuation friction and contact that affect a modeling scheme the most. Few of these studies include pathways to incorporate them into their already complicated models and instead rely on a point contact assumption.

The effect of a soft outer shell on a robot has a significant impact on its dynamics. A soft outer shell of the robot can be used for absorbing impacts when rolling across unknown terrain and allowing for a smoother ride [9]. Dravid studied a similar robot and found that inflation pressure has a noticeable effect on the overall power output of the system, but did not give an explicit model of its exact effects [10]. Other researchers have designed specialized compensation terms to account for any soft shell effects, but do not explicitly attempt to model the outer shells' rolling dynamics [11]. In developing a modeling scheme, the impacts of the soft outer shell cannot be ignored.

Featherstone published a landmark work on methods for numerically acquiring a system's rigid body dynamics through a set of algorithms [12]. Such techniques have been incorporated into many popular robotics toolboxes. Most share the common feature of parsing the rigid body dynamics from a supplied URDF file to allow researchers the ability to study the numerical response of the robot's equation of motion. Drake and SOFA are two such implementations of Featherstone's work, yet they include additional functionality to model soft contact dynamics beyond rigid body properties. Drake's hydroelastic contact model uses pressure fields to approximate the contact area and resulting forces [13]. SOFA is geared toward modeling the whole bodies of soft robots of all shapes through Finite Element methods [14]. The outer shell of a spherical robot is usually the only component that is soft, and its spherical geometry lends itself to Drake's lighter-weight version of a contact model. A side-by-side comparison of our physical robot and its digital twin in Drake is shown in Figure 1.

This paper will outline our approach to systematically modeling a soft pendulum-driven spherical robot. The robot's rigid body dynamics will be numerically generated using Drake's implementation of Featherstone's rigid body dynamics algorithms through a custom URDF file for a spherical robot. Methods for characterizing the frictional losses in

Manuscript received: May 07, 2025; Revised August 14, 2025; Accepted September 24, 2025.

This paper was recommended for publication by Editor Cecilia Laschi upon evaluation of the Associate Editor and Reviewers' comments.

Research supported by the Texas A&M Chancellor's Research Initiative and matching funds from the Texas Governor's University Research Initiative.

[1] Authors are with Texas A&M University, College Station, TX, USA

[2] Author is with Belmont University, Nashville, TN, USA

Digital Object Identifier (DOI): see top of this page.

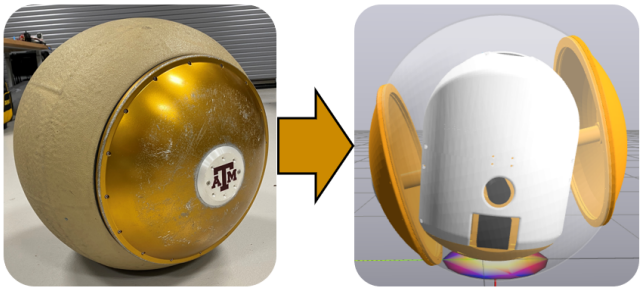

Fig. 1. A soft spherical robot and respective experiment using Drake's contact model

the two actuated degrees of freedom of the robot will be shown for model completeness. Three different models for the soft outer shell will be introduced, one based on Drake's native hydroelastic contact model, another for linear injected dynamics, and a regular point contact case for control. These models will be tuned against empirical data to match the dynamic frequencies and damping ratios in the steering direction. A simple parameter sensitivity study for the hydroelastic parameters will also be introduced. Finally, the tuned models will be tested in a dynamic experiment of the robot rolling down a ramp to assess the models' ability to follow the driving direction.

II. Modeling Approach

Based on work introduced in Featherstone [12], the forward dynamics of a rigid body system are given in the form of equation (1), where $H(q)$ is an inertia matrix, C is a matrix that depends on the state positions and velocities q or a vector of external forces f^x if any. These equations are typically found and integrated by hand, or Drake can generate the numerical system by parsing a properly designed URDF.

$$\tau = H(q)\ddot{q} + C(q, \dot{q}, f^x) \tag{1}$$

Figure 2 presents a flowchart for our modeling framework. In the figure, a rigid body dynamic model is connected to joint friction losses and external forces. The friction losses are in series with the control effort on the actuated joints, and additional dynamics from the soft shell models are implemented through external spatial forces, f^x. The simulated states are then fed to a graph, data file, or Drake's Meshcat visualizer for analysis or comparison to experimental data.

A. URDF Model

Drake uses a URDF as a starting point for deriving the system dynamics. Obtaining an accurate file is trivial for common robots thanks to a recent database compiled by Tola and Corke [15]. Their database includes many robot arms, dogs, and humanoids; however, it lacks a URDF for any spherical robot, so we created our own. The accuracy of the URDF will translate to the accuracy of (1).

A SolidWorks assembly already existed to design and manufacture parts for our hardware testbed. To create an accurate URDF, the mass values of all individual components were updated, and corresponding colors were applied. With

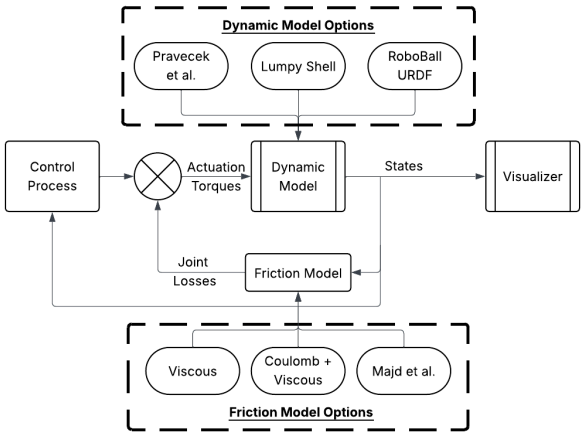

Fig. 2. Flowchart of Drake environment with modular modeling framework

this information, the SolidWorks' Mass Analyzer tool was used to approximate the inertia and the center of mass of the various links based on the components' relative positions and masses. Some of them were slightly off the center axis, highlighting an advantage of this approach. Using URDF-based models allows for the easier capture of slight inertial imbalances in the dynamic model. The export of frames, masses, and meshes was handled with the Solidworks2URDF ROS tool; a selection of these values can be found in Table II at the end of this document.

The robot consists of three key parts: the Pendulum, the Pitch Center, and the outer shell. The outer shell consists of both soft and rigid components. The Bedliner link represents the soft outer shell and primary soft contact point between the robot and the world. The Pipe Assembly contains the robot's driveshaft and connects the bedliner to the rest of the robot. The Pitch Center and Pendulum links make up the 2-degree-of-freedom pendulum, the primary control mechanism. These links can be visualized in the kinematic model on the left of Figure 3.

The exported URDF consists of a two-branch floating body structure. The Pitch Center is the kinematic tree's root and sits between the pendulum and two outer shell links. A 6-DOF floating joint connects it to the simulation inertial or world frame. The shell is split into the Pipe Assembly and Bedliner links, which are fixed together. Drake-specific tags are later applied to the Bedliner collision properties to register it as soft. This topology is shown on the right of Figure 3, next to the kinematic visual model.

State Names: To validate the proposed models in the following sections, measured robot state data will be compared against simulated data. These states are illustrated in Figure 4 and will be called the pendulum angle, θ, and the pipe angle, ϕ, respectively. The pendulum angle is the angle between the pendulum and driveshaft in the steer direction or the revolute joint (steer axis) value in the URDF. The pipe angle is the angle the pipe assembly makes with the ground. This is found from the roll angle in an Euler angle interpretation of the base floating joint. τ_s is the net torque acting on the

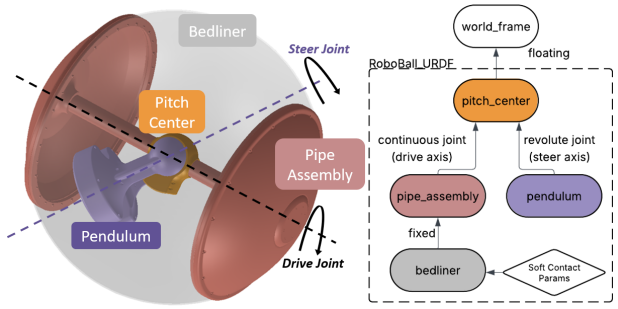

Fig. 3. Robot URDF kinematic structure and topology

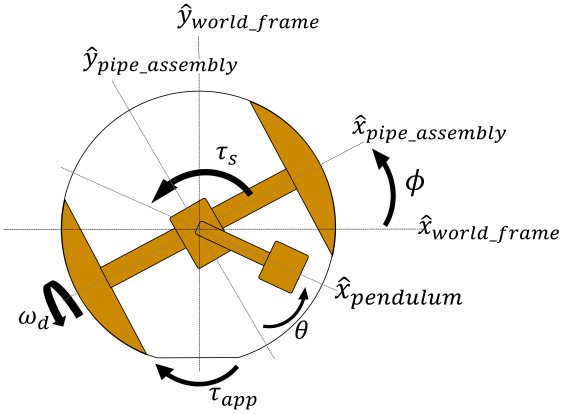

Fig. 4. Robot State Diagram

steer axis; this is the same Actuation Torque called out in Figure 2. The symbol τ_{app} represents the additional contact forces a spherical soft shell has on the outer Bedliner and Pipe Assembly links. The drive velocity of the robot is the angular speed of the pipe assembly about its $\hat{x}$ axis, denoted by ω_d.

B. Joint Friction Models

URDF format only natively supports proportional damping. However, more detailed models can be implemented through Drake's LeafSystem abstraction layer. This abstraction is shown in Figure 2, where the dynamics are wired into the system through input torques at the simulated actuators (τ_s). This will mimic frictional losses in the gear reductions on the robot's motor.

Three different models were implemented and compared against experimental data from the robot. All three models follow a structure of taking in the joint's velocity, v, and yielding some resisting torque as an output, $\tau_{friction}$. As a control, the first model is the standard viscous damping natively handled by the URDF, shown in (2) with the static and dynamic coulomb parameters set to zero $\mu_s, \mu_d = 0$ with a viscous coefficient c. The outcome of this is shown in Figure 7 as the Viscous. Tuning μ_s, μ_d to non-zero values is the Coulomb+Viscous model.

$$\tau_{friction} = \begin{cases} \mu_s \text{sign}(v), & \text{if } v < tol \\ -\mu_d \text{sign}(v) - cv & \text{otherwise} \end{cases} \quad (2)$$

The third model was derived by Majd et al. to handle stiction in servos and is presented at equation (6) from [16] but repeated in (3) below. This model includes additional terms for tuning the modeled response, which are $[f_\omega, f_c, \sigma, \omega_c, n]$. All three models were tuned to the steer response of the robot with a 15:1 reduction, and the output torques are shown in Figure 5.

To collect data to tune the friction models, our physical robot was placed in a testing stand that locked its outer rolling mode in the steer direction. This isolated the inner steer joint of the pendulum to study the decaying effect of the pendulum's swing due to the gearing's friction. Figure 6 shows the pendulum in the test stand and its rendering in Drake's Meshcat.

$$\tau_{friction} = f_\omega v[f_c + \sigma e^{-|v/\omega_c|} - (\sigma + f_c)e^{-|nv/\omega_c|}]\text{sign}(v) \quad (3)$$

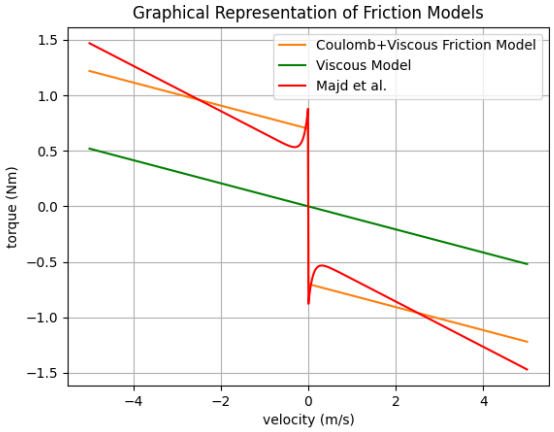

Fig. 5. Comparison of output torque responses of various velocity-based friction models

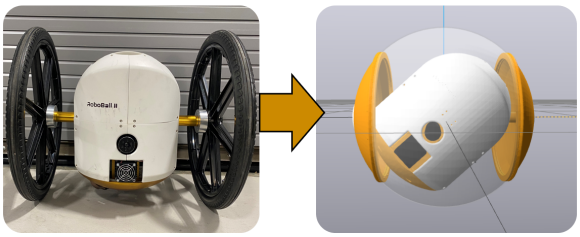

Fig. 6. Robot in a stand to isolate its steer joint with its respective digital twin in MeshCat

Of the tested models, Majd's model fit the best in the steering direction, so it was the only model fitted in the drive direction with a 33:1 reduction. The resulting friction models were then overlaid over the robot's data and shown in Figures 7 and 8.

This section outlined the modeling efforts to capture the dynamic effects of the joint losses of the robot. In the final tests of the paper, where the robot rolls down a ramp, both axes will be free to move under these dissipative effects as

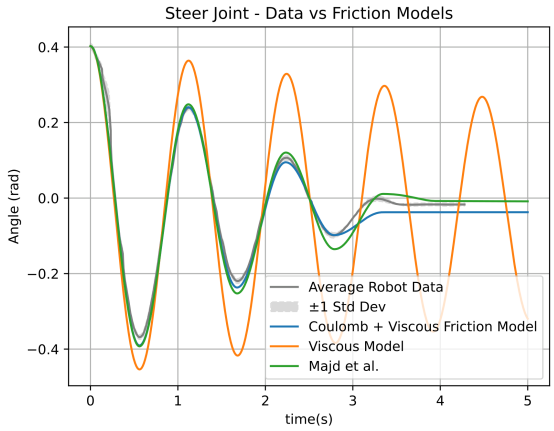

Fig. 7. Experimental data of the robot's steer axis overlaid with model output with different friction models

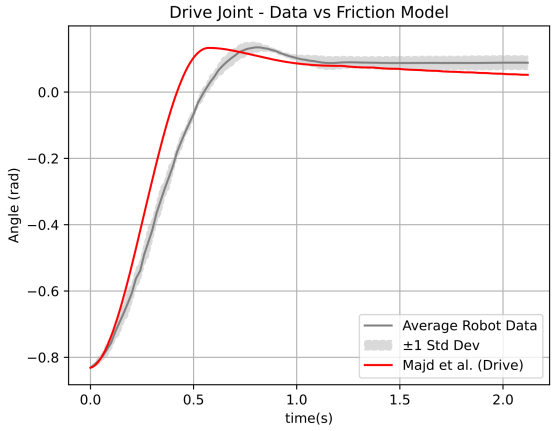

Fig. 8. Experimental data of the robot's drive axis overlaid with a fitted Majd model

defined by Majd. The parameters for each tuned model are given in Table I.

TABLE I
PARAMETERS FOR JOINT FRICTION MODELS

Model	Parameters	Values
Viscous	c	0.104
Viscous + Coulomb	μ_s, μ_d, c	[0.7, 0.65, 0.104]
Majd - Steer	f_w, f_c, σ, ω_c, n	[0.20, 0.45, 10, 0.1, 1]
Majd - Drive	f_w, f_c, σ, ω_c, n	[1.78, 1.24, 8.33, 1.36, 1.60]

III. OUTER SHELL CONTACT MODELS

The next non-conservative aspect of the robot is its outer shell. This section details an experiment to isolate the shell dynamics from the internal pendulum using a physical clamp. Then, a detailed model that injects additional stiffness and dissipation terms as external forces to model the shell will be presented with our implementation of Drake's hydroelastic model. The models will be compared against a typical point contact assumption as a control model.

A. Experimental Shell Dynamics in Steering Direction

To initially estimate the effects of the robot, we designed a clamp to lock the steering axis of the shell, shown in Figure 9.

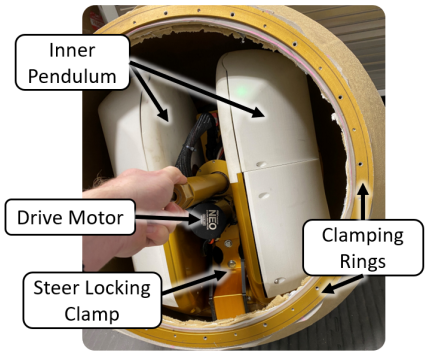

Fig. 9. Reinforced 3D printed clamp to lock the steering.

This clamp removes the random motions of a free-falling pendulum and reduces the system to the equivalent dynamics of a rolling half cylinder. Dynamically, this constrains the relative motion of the pendulum relative to the pipe assembly such that $\theta = 0$ in Figure 4. The linearized equation is stated below and can be derived using typical Lagrangian methods with appropriate transforms to represent all dynamic link masses and inertia in the Pipe Assembly frame.

$$M_{eq}\ddot{\phi} + K_{eq}\phi = \tau_{app} \tag{4}$$

Where $m_i, r_i,$ and I_i are the mass, center of mass position, and inertia of the Pendulum, Pitch Center, and Pipe Assembly Links, respectively ($i = p,\ pc,\ s$). R is the nominal outer radius.

$$M_{eq} = (I_{eq} - 2(m_{pc}r_{pc} + m_p r_p)R)$$
$$I_{eq} = I_s + (I_{pc} + m_{pc}r_{pc}^2) + (I_p + m_p r_p^2) + m_{total}R^2$$
$$K_{eq} = (m_{pc}r_{pc} + m_p r_p)g$$

Equation (4) is a simple harmonic oscillator in the rotational coordinate of ϕ. To investigate how well the equation models the robot with locked steering, we manually adjusted the robot to an offset angle and released it. This was repeated at different pressures, and the resulting traces were processed to obtain the damping ratios and natural frequencies in the steering direction. The resulting values are plotted in Figure 10 along with appropriate exponential and linear regressions for the damping ratio ζ and damped frequency ω_n. If the system were accurately represented by (4), then the system's frequency should be given by equation (5)

$$\omega_n^2 = \frac{K_{eq}}{M_{eq}} \tag{5}$$

This value is invariant to pressure, so it is shown at the bottom of Figure 10 as a dashed line. Numerical values from the URDF for each symbol are presented in Table II at the end of this document.

When the parsed dynamic model of the URDF is simulated in a point contact case there are no additional contact forces applied to the rolling system ($\tau_{app} = 0$). In this case, equation (4) and a Drake model with locked steering under point contact are equivalent. The resulting frequency and ratios are shown in Figure 10, where the system aligns with the calculated frequency and there is no damping. This is not close to the empirically measured results, so the softness of the outer shell affects the dynamics in this steering direction.

B. Injected Contact Dynamics

This section will derive a model to inject additional dynamics into the model to account for the discrepancies from the soft shell. Writing equation (4) in terms of the standard form of second-order ODEs. In the equation, both frequency, ($\omega_n(p)$), and damping ratio, ($\zeta(p)$), are functions of pressure, p. These relationships are derived from an exponential and linear regression of rolling data shown in the boxes of Figure 10.

$$\ddot{\phi} + 2\zeta(p)\omega_n(p)\dot{\phi} + \omega_n(p)^2\phi = \tau_{app} \tag{6}$$

By equating the coefficients of (4) and (6), we can recover relationships for additional stiffness and damping terms that can be injected into the system through applied forces to account for the dynamic effects of the soft shell as a function of pressure.

$$K_{inject}(p) = \omega_n(p)^2 M_{eq} - K_{eq} \tag{7}$$
$$C_{inject}(p) = 2M_{eq}\omega_n(p)\zeta(p) \tag{8}$$

We can then formulate an expression to inject the dynamics into the system through applied forces, τ_{app}. We will refer to equation 9 as the injected shell dynamics.

$$\tau_{app} = -C_{inject}\dot{\phi} - K_{inject}\phi \tag{9}$$

The injected stiffness and damping move the system closer to the experimental values. The natural frequencies line up, but (8) underapproximates the experimental damping values, possibly due to additional non-linear dissipative effects from the inflatable soft shell that are not captured through the linear systems identification.

C. Hydroelastic Contact

As an additional contact model, Drake's built-in hydroelastic contact model was implemented in this scenario. Initially developed to represent compliance in soft robotic grippers, existing tuning guidelines are primarily targeted at manipulators, and the model introduces compliance and dissipation only in the vertical direction. Consequently, we do not expect it to contribute additional stiffness to the rolling dynamics. However, because the normal velocity flux of a sphere rotating through a cross-section is non-zero, the model can still capture some rolling-induced dissipation. The hydroelastic model requires two parameters: an elastic modulus and a dissipation coefficient. The elastic modulus, m_{hydro}, represents the expected deformation (or contact "flat") of the robot and was estimated following Drake's recommended procedure, given in (10), where f_n is the normal force of the robot (its weight) and V is the estimated intersecting volume between the undeformed sphere and a flat surface. This contact volume is pressure-dependent and was derived from prior measurements on a similar robot reported in Section IV of [17]. For an initial guess of the dissipation, we chose the coefficient as C_{inject} from (8). The results are shown in Figure 10, where using C_{inject} as the dissipation coefficient overestimates the damping in the hydroelastic case.

$$m_{hydro} = \frac{f_n}{V(p)} \tag{10}$$
$$d_{hydro} = C_{inject} \tag{11}$$

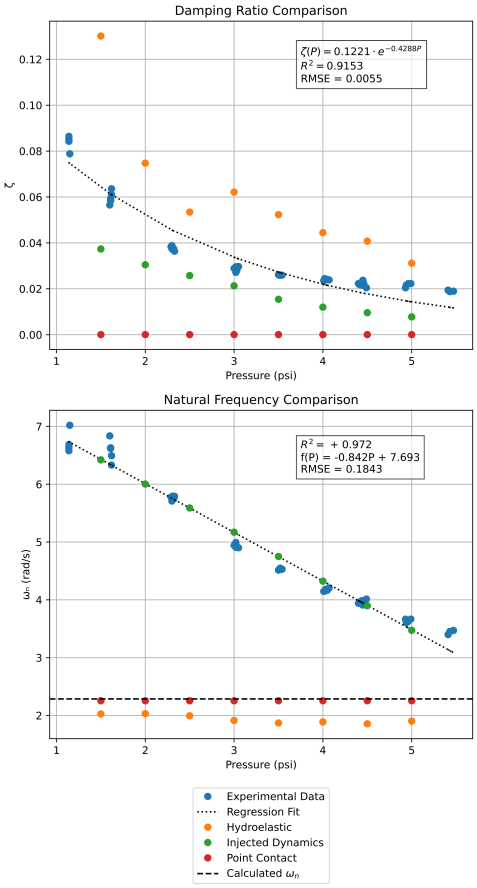

Fig. 10. Empirical Results of Isolated Shell Dynamics Testing

From this shell dynamic tuning process, the shell has a significant effect on the overall system's dynamics. The model presented in (8) provides the best fit without additional modifications. Still, it only exists in the steering plane of the robot, whereas the hydroelastic model derives from mesh collisions and would be suitable for all rolling directions.

D. Hydroelastic Parameter Sensitivity

The values for the two hydroelastic parameters, the modulus and dissipation (m and d), were chosen to vary with

pressure along the models presented in (10) and (8). This section will outline a parameter sensitivity study to determine the best way to continue to tune the parameters.

The previously calculated values at each pressure are used as a control point, increasing or decreasing either the modulus or dissipation by 50% to observe the change in the simulated damping ratio. The resulting damping ratio response is shown in Figure 11 with associated percent changes in error in the context of the original.

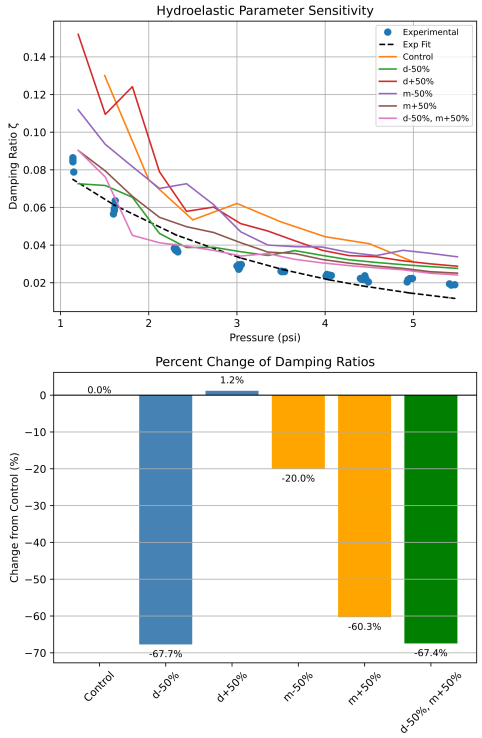

Fig. 11. Parameter Sensitivity Study of Hydroelastic Model

From the figure, decreasing the dissipation and increasing the modulus both decreased the percent error from the control. However, applying both together did not yield additional benefits. We will use the hydroelastic model with a 50% reduction in the dissipation for the analysis in the next section.

IV. Modeling the Full Dynamics Through Uncontrolled Descent

The previous sections detailed the derivation of models for the isolated non-conservative aspects of the robot. In this section, the models for joint friction and shell dynamics are combined with the Drake rigid body engine to model the robot rolling down a ramp at different pressures. For this experiment, the pendulum is unconstrained and subjected to the frictional losses specified by the respective Majd model (Shown in Figures 7 and 8). The only change from the steering to the drive direction is dropping the $K_{injected}$ term from (9) and $\dot{\phi}$ is replaced with the pipes rolling velocity, ω_d.

In each test, the robot is inflated to a target pressure, then released from rest at a marked spot on a ramp. The robots' drive speed, as well as pendulums and pipe angles, were recorded. The experimental data were used to set the initial pipe angle and appropriate contact parameters at a certain pressure of the robot before it was released from rest. A side-by-side view of the experimental setup and virtual recreation of it is shown in Figure 12.

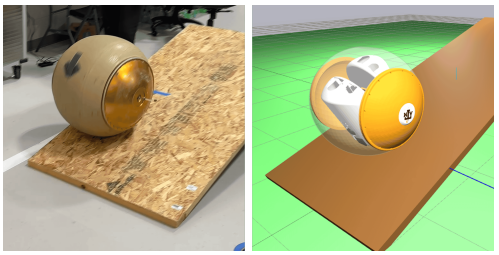

Fig. 12. Robot rolling down a ramp and its respective digital twin in meshcat

When the robot leaves the ramp, an additional step disturbance is introduced to the system that this method does not model. This would impact any dynamic response as it transitions. To simplify the analysis, only data from before the robot left the ramp was considered, omitting the transition zone and the period when the robot left the ramp. The simulated velocity data is subtracted from the measured velocity data at each sample time, such that overestimated models are positive. This Point Mean Error (PME) is shown in equation 12 where the subscripts for the experimental and simulated drive angular velocity are e and s, respectively. Figure 13 shows the resulting PME from each run at the tested pressure for the three different contact models.

$$PME = \frac{1}{N}\sum_{i=0}^{N}\frac{(\omega_e(i) - \omega_s(i))}{\omega_e(i)} \times 100\% \qquad (12)$$

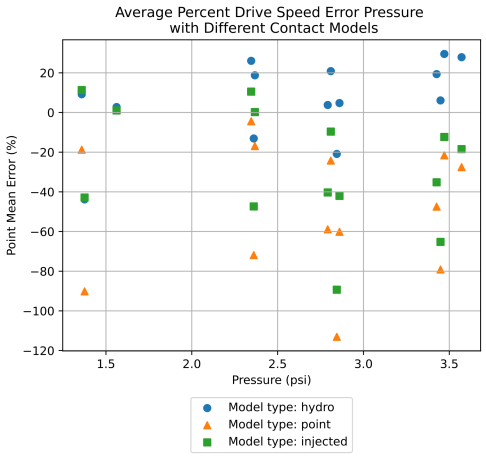

Fig. 13. Drive speed errors at each pressure

Figure 14 averages the PME from all pressures at each model for an overall metric.

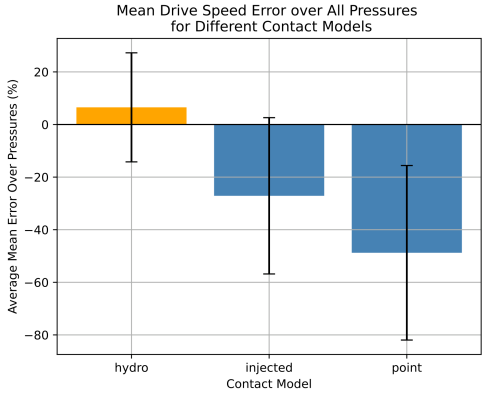

Fig. 14. Averaged drive speed error overall pressures

For this case, the tuned hydroelastic model was able to predict the experimental drive velocity more accurately on average than the injected or point contact models. While slightly underestimated, the model is overdamping the system, and in line with the trend from the previous section, where reducing the dissipation from the calculated C_{inject} yielded better results. However, both the injected and hydroelastic models were an improvement compared to a rigid body point contact assumption.

V. Discussion and Model Limitations

While the tuned hydroelastic model is accurate and exceeds regular point contact models, its capabilities are limited. The hydroelastic representation does not model the deformations in a flexing body and ignores any extra stiffness the flexing may introduce in the rolling direction. The software must also set the contact parameters before running the simulation, so that this architecture cannot model changes in pressure during a simulation period.

VI. Conclusion

This letter presents an empirically validated, modular dynamic modeling framework for a soft, pendulum-driven spherical robot. The approach leverages Drake's URDF-based rigid-body engine and augments it with interchangeable modules for joint friction and soft-shell contact dynamics. Three friction models were tuned to characterize internal joint losses. In addition, the outer shell was represented using three alternative contact models, including the hydroelastic method and a pressure-dependent injected stiffness–damping formulation. Experimental isolation of the steering dynamics enabled direct parameter tuning, and ramp descent tests demonstrated that tuned models could be used in the driving direction as well.

TABLE II

Measured Numerical Values

Parameter Set	Symbols	Values
Link mass (kg)	$m_{pc},\ m_p,\ m_s$	$[2.77, 22.03, 16.53]$
Link Inertias (kgm^2)	$I_{pc},\ I_p,\ I_s$	$[1.8e^{-2}, 4.4e^{-1}, 1.04]$
Distance measures (m)	$r_{pc},\ r_p,\ R$	$[0.05, 0.095, 0.305]$
Ramp Angle		16^o

References

[1] Wei Ren et al. "Spherical robot: A novel robot for exploration in harsh unknown environments". In: *IET Cyber-Systems and Robotics* 5.4 (2023), e12099.

[2] Rishi V. Jangale et al. "Scaling of RoboBall: A Parametric Robot Family for Crater Exploration". In: *2025 IEEE Aerospace Conference*. 2025, pp. 1–8. DOI: 10.1109/AERO63441.2025.11068434.

[3] Matthew R Burkhardt et al. "Energy harvesting analysis for moball, a self-propelled mobile sensor platform capable of long duration operation in harsh terrains". In: *2014 IEEE international conference on robotics and automation (ICRA)*. IEEE. 2014, pp. 2665–2672.

[4] Aminata Diouf et al. "Spherical rolling robots—Design, modeling, and control: A systematic literature review". In: *Robotics and Autonomous Systems* 175 (2024), p. 104657.

[5] "Gregory Schroll". ""Model of Spherical Robot from First Principles"". MA thesis. "Colorado State University", 2009.

[6] Matt Burkhardt and Joel W. Burdick. "Reduced dynamical equations for barycentric spherical robots". In: *2016 IEEE International Conference on Robotics and Automation (ICRA)*. 2016, pp. 2725–2732. DOI: 10.1109/ICRA.2016.7487434.

[7] Xiaoqing Guan et al. "An Online System Identification Algorithm for Spherical Robot Using the Koopman Theory". In: *IEEE Robotics and Automation Letters* 10.5 (2025), pp. 4644–4651. DOI: 10.1109/LRA.2025.3552997.

[8] Guelis Montenegro et al. "Modeling and control of a spherical robot in the CoppeliaSim simulator". In: *Sensors* 22.16 (2022), p. 6020.

[9] Faranak Davoodi, Joel W Burdick, and Mina Rais-Zadeh. "Moball network: a self-powered intelligent network of controllable spherical mobile sensors to explore solar planets and moons". In: *AIAA SPACE 2014 conference and exposition*. 2014, p. 4261.

[10] Meghali Prashant Dravid et al. "Design of a Soft Shell for a Spherical Exploration Robot Traversing Varying Terrain". In: *2024 IEEE/RSJ International Conference on Intelligent Robots and Systems (IROS)*. 2024, pp. 10939–10944. DOI: 10.1109/IROS58592.2024.10802644.

[11] Derek J. Pravecek et al. "Empirically Compensated Setpoint Tracking for Spherical Robots With Pressurized Soft-Shells". In: *IEEE Robotics and Automation Letters* 10.3 (2025), pp. 2136–2143. DOI: 10.1109/LRA.2025.3527308.

[12] Roy Featherstone. *Rigid body dynamics algorithms*. Springer, 2014.

[13] Russ Tedrake and the Drake Development Team. *Drake: Model-based design and verification for robotics*. 2019. URL: https://drake.mit.edu.

[14] François Faure et al. "Sofa: A multi-model framework for interactive physical simulation". In: *Soft tissue biomechanical modeling for computer assisted surgery*. Springer, 2012, pp. 283–321.

[15] Daniella Tola and Peter Corke. "Understanding URDF: A Dataset and Analysis". In: *IEEE Robotics and Automation Letters* 9.5 (2024), pp. 4479–4486. DOI: 10.1109/LRA.2024.3381482.

[16] V.J. Majd and M.A. Simaan. "A continuous friction model for servo systems with stiction". In: *Proceedings of International Conference on Control Applications*. 1995, pp. 296–301. DOI: 10.1109/CCA.1995.555719.

[17] Micah Oevermann et al. "RoboBall: An All-Terrain Spherical Robot with a Pressurized Shell". In: *2024 IEEE International Conference on Robotics and Automation (ICRA)*. IEEE. 2024, pp. 13502–13508.